Contents lists available at ScienceDirect

Thermal Science and Engineering Progress

journal homepage: www.elsevier.com/locate/tsep



Full-spectrum *k*-distribution weighted sum of gray gases model for air and oxyfuel combustion of hydrogen-hydrocarbon blends at atmospheric pressure

Johannes Losacker*, Alex M. Garcia, Nico Schmitz, Christian Wuppermann

RWTH Aachen University, Department for Industrial Furnaces and Heat Engineering (IOB), Kopernikusstraße 10, Aachen, 52074, Germany

ARTICLE INFO

Dataset link: WSGGM Implementations (Origina 1 data)

Keywords:
Weighted sum of gray gases
WSGG
Hydrogen
Ammonia
Biogas
Gas radiation

ABSTRACT

In the context of decarbonization of heating processes, alternative fuels as hydrogen, ammonia, or biogas are explored to substitute conventional fuels as natural gas. The altered flue gas compositions from such flames demand flexible modeling of radiative properties of the participating gases $\rm H_2O$ and $\rm CO_2$. Various Weighted Sum of Gray Gases (WSGG) model formulations and coefficients have been proposed in the literature, but few cover all conditions that result from the combustion of any blend of the aforementioned fuels. In this work, two sets of coefficients for a WSGG model with 5 gray gases are calibrated for air and oxyfuel combustion conditions at atmospheric pressure, to improve on the accuracy and flexibility of existing models. Weights and absorption coefficients are derived from k-distributions based on line-by-line integrations using the HITEMP 2010 spectroscopic database. Base functions are fitted to continuously recover the weights and absorption coefficients within the range of calibration. The new model covers $\rm H_2O$ to $\rm CO_2$ molar ratios of $\rm 1 \le Mr \le \infty$, and temperatures in the range of 300 K $\rm \le T \le 2700~K$ for air combustion, and 300 K $\rm \le T \le 3000~K$ for oxyfuel combustion. The models are assessed by predictions of total emissivity as well as radiative heat flux and source term in a 1D slab. Benchmark solutions are obtained from line-by-line integrations covering the compositions of the calibration database. The new model shows significantly improved predictions in comparison to recent WSGG models.

1. Introduction

In numerical simulations of high-temperature processes, the accurate prediction of heat transfer is crucial to the results. At operating temperatures exceeding 1000 K, radiative heat transfer can account for over 80% of the heat transferred to the process in industrial furnaces [1,2], making it the predominant heat transfer mechanism. In cases where the heat is released by combustion, the flue gas that is occupying the furnace participates in radiative heat transfer. Therefore, a key modeling task is determining the gas properties that characterize the interaction via absorption and emission.

A first distinction between gas radiation models can be made by the treatment of the spectral dependency of radiative properties. The most accurate numerical method is to compute the spectrum considering each spectral line and solve the radiative transfer equation (RTE) for the intensity carried at sufficiently narrow wavenumber intervals. Such procedure is referred to as line-by-line (LBL) integration. As latest databases list more than 10^8 spectral lines for H_2O [3], this method

is computationally too expensive to be employed in most engineering applications [4]. The highly resolved databases are rather used to deduce simplified models, trading spectral information for reduced computational cost. Band models reflect the spectral behaviour to some extent, as they use spectral absorption coefficients representing wavelength intervals. Depending on the bandwidth and spectral coverage they are classified as narrow-, wide-, or full spectrum band models [4]. At only a fraction of the computational cost, these models can be in close agreement with the line-by-line method. For many applications as industrial furnaces however, the spectral information is of minor importance and the prediction of the overall radiative heat flux is sufficient. This can be provided by the yet computationally cheaper approach of global models as the Weighted Sum of Gray Gases (WSGG) model [5], where the spectral dependencies are not considered and only the radiative heat flux is recovered. Due to the efficiency and flexibility, the WSGG model is the most popular model to treat nongray combustion media [6]. The model can be used with arbitrary RTE solution methods [7] and a good trade-off between computational cost and accuracy is reported for the use in combustion applications [8].

E-mail address: losacker@iob.rwth-aachen.de (J. Losacker).

^{*} Corresponding author.

Table 1
Summary of recent WSGG models for H_2O-CO_2 -mixtures with number of non transparent gray gases N_g , calibrated ranges of molar ratio Mr and temperature T and underlying database. A list of molar ratios indicates one set of coefficients calibrated per molar ratio; ranges of molar ratio indicate a continuous model formulation. Authors printed in bold published their coefficients.

Authors	Year	$N_{ m g}$	Mr	T[K]	Reference
Bahador et Sunden [11]	2008	3	1,2	500-2500	LBL
Krishnamoorthy [12]	2010	5	2, 3	1000-2000	Empir. Correlations
Yin et al. [13]	2010	4	0.125, 0.25, 0.5, 0.75, 1, 2, 4	500-3000	EWB
Johansson et al. [14]	2011	4	0.125–2	500-2500	SNB
Rehfeldt [15]	2011	4	0.056-2.167	600-2400	EWB
Kangwanpongpan et al. [16]	2012	4	0.125-4	400-2500	LBL
Dorigon et al. [17]	2013	4	1, 2	400-2500	LBL
Krishnamoorthy [18]	2013	4	0.11, 0.5, 1, 2	1000-2000	SNB
Bordbar et al. [19]	2014	4	0.01–4	500-2400	LBL
Guo et al. [20]	2015	4	0.05-2	600-2500	LBL
Shan et al. [21]	2018	4	0.125-4	500-2500	SNB
Coelho et Franca [22]	2018	4	2	400-2500	LBL
Wang and Xuan [23]	2019	5	1	500-2500	LBL
Bordbar et al. [24]	2020	4	0-∞	300-2400	LBL
Wu et al. [25]	2021	4	0.01-4	400-3000	LBL
Xu et al. [26]	2021	5	3, ∞	400-2500	LBL
Zhou et al. [27]	2023	4	2.25, 3, 4, 4.5	400-2500	SNB
Liu et al. [28]	2023	8	0.05–4	300–2500	LBL

In the combustion of hydrocarbon fuels, the most abundant flue gas species that participate in radiative heat transfer are CO2 and H2O. Extensive research has been dedicated to extend and improve the WSGG model for mixtures of these species. One approach to deal with the two participating species is the so called double integration approach, that was followed for instance by Cassol et al. [9] in their model for arbitrary CO2-H2O mixtures. Weighted gray gas representations are derived for each single specie and the mixture weights and absorption coefficients are found from multiplication of each possible weight combination while the respective absorption coefficients are added. The resulting number of weighted gray gases of the mixture is significantly increased compared to the single species gases. As the number of gray gases is proportional to the computational expense of the model, it is common practice to treat the mixture as a single gas instead and introduce the H_2O to CO_2 molar ratio $Mr = p_{\rm H2O}/p_{\rm CO2}$ as a variable on which the model parameters depend. While this approach can provide comparable accuracy at reduced computational cost, it is not as straight forward to apply on arbitrary mixture compositions [10]. Coefficients are fitted to hold within a certain range of molar ratio, temperature, and pressure. A model that is calibrated to cover a too wide range of conditions is penalized with either increase of complexity or loss of accuracy. Consequently, numerous model formulations and calibrated coefficients have been proposed depending on the intended application. Recent models are listed in Table 1 together with the number of non transparent gray gases, ranges of molar ratio and temperature, and the underlying reference database.

Model coefficients are either tailored to hold in vicinity of discrete molar ratios [11,13,17,18,22,23,26,27], or a continuous formulation for varying molar ratios is given [14-16,20,21,24,25,28]. The latter option has the advantage, that only a single set of coefficients is required, simplifying the implementation for cases with non-homogeneous gas compositions. The majority of the listed models cover molar ratios up to 4 or less, usually aimed on combustion of coal, liquid hydrocarbon fuels, and natural gas. Only Bordbar et al. [24] provide continuous formulations for molar ratios beyond 4 and up to pure H2O, which occurs at the combustion of H2 or NH3. Besides modeling mixtures of CO2 and H2O, efforts have been made to include soot [9,28] and CO [25] as an additional participating medium. Due to the pressure broadening of spectral lines, which is especially pronounced in case of H2O, the species partial pressure has a non-linear effect on total emissivity and restricts the applicability at pressures deviating from the fitting conditions. To overcome this limitation, similar to the treatment of varying molar ratios, some authors provide different coefficients at discrete partial pressures [10,13,22], while others introduce partial or total pressure as variables to formulate their models [21,23,26]. The

temperatures at which the models are calibrated range from $300\,\mathrm{K}$ to $3000\,\mathrm{K}$. Temperatures above $2500\,\mathrm{K}$ are covered only by the models of Yin et al. [13] and Wu et al. [25], both valid up to $3000\,\mathrm{K}$.

While earlier WSGG models also used empirical correlations, exponential wide band (EWB) models, and spectral narrow band (SNB) models for calibration, more recent models rely on line-by-line integrations based on highly resolved spectroscopic databases. Most models are fitted to recover total emissivity within the calibration range of temperature, composition, pressure and pressure path length. In contrast, the models proposed by Guo et al. [20] and Liu et al. [28] are developed from full spectrum k-distributions. Under the assumption of a correlated absorption coefficient, the model parameters are derived directly from the spectra in such a way that each gray gas represents the same wavenumber interval at any gas state. Such derived gray gases have actual physical significance, as the radiative energy carried at each gray gas is kept within the same wavenumber interval. Consequently, this approach has a conceptual advantage compared to the fitting on total emissivity when applied on non-homogeneous cases. Moreover, the uncertainties of the numerical fitting on total emissivity are avoided.

The choice of a WSGG model for a combustion application is driven by the state of the flue gas in terms of pressure, temperature, and composition. The latter results from the composition of fuel and oxidant. In the course of decarbonization of energy-intensive industries, recent research is dedicated to substitute conventional hydrocarbon fuels by renewable fuels for industrial furnaces in the sectors of steel [29], aluminium [30], and glass production [31]. As these fuels might not be available in sufficient quantities to allow complete substitution in the near future, the use of fuel blends is expected to play an important role in facilitating the transition to carbon-free heating processes [32]. Another option to reduce CO2 emissions is the reduction of fuel consumption in the first place by improving process efficiencies. This may be achieved by the use of oxyfuel, where oxygen is employed as the oxidant instead of air. In this case, N2, which is not contributing to the heat release, is not present in the flue gas, yielding higher combustion temperatures and increased efficiency [33].

The partial pressures of $\rm H_2O$ and $\rm CO_2$ and their molar ratio in flue gas of stoichiometric combustion of some reference fuels with air and oxyfuel at atmospheric pressure are given in Fig. 1. Complete combustion of methane yields a molar ratio of Mr=2 in the flue gas. Considering longer chain hydrocarbon fuels, the molar ratio is decreased, octane combustion for instance yields a molar ratio of Mr=1.125. Combustion flue gas of an exemplary biogas consisting of 50% $\rm CO_4$ and 50% $\rm CO_2$ by volume has equal contents of $\rm H_2O$ and $\rm CO_2$, and hence, a molar ratio Mr=1. For fuels that do not contain carbon, as $\rm H_2$ or $\rm NH_3$, the $\rm CO_2$ content vanishes and the molar ratio approaches

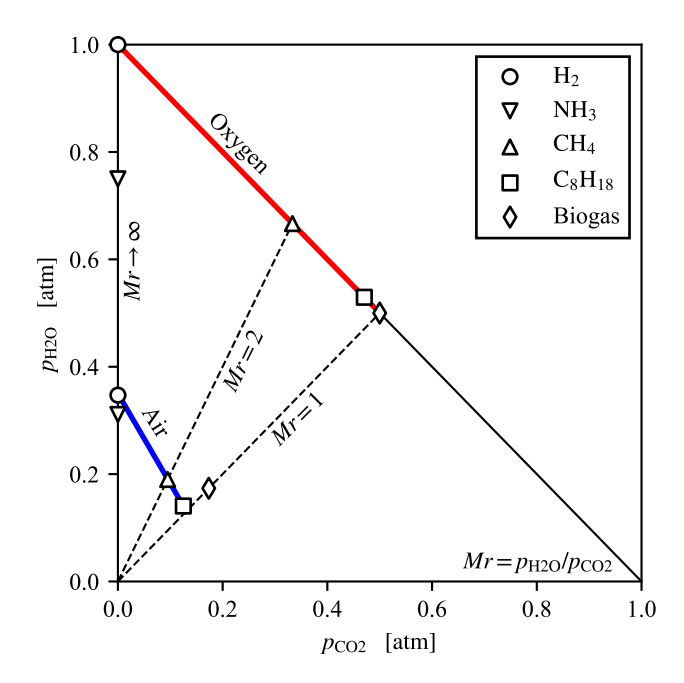


Fig. 1. $\rm H_2O$ and $\rm CO_2$ partial pressure and molar ratio for stoichiometric combustion of different fuels with air and oxygen at atmospheric pressure.

infinity. In case of fuel blends, the resulting molar ratio is found in between the values of the pure fuels. Considering oxyfuel instead of air combustion, the flue gas dilution by N_2 is eliminated, resulting in higher concentrations of H_2O and CO_2 , while the molar ratio is not affected.

Given an industrial furnace that operates on fuel blends, or even different fuels per burner, resulting in non-homogeneous flue gas compositions within a single domain, it is convenient to employ a model which covers all conditions given in Fig. 1. From analysis of published WSGG models it is found that except for double integration models, only the mixture model of Bordbar et al. [24] provides a continuous formulation for Mr > 4. However, the extension of the model to Mr > 4conditions is realized by linear interpolation of weights and absorption coefficients between the values calibrated at Mr = 4 and $Mr = 10^8$, rather then being supported by calibration at intermediate compositions. Additionally, the range of temperatures up to 2400 K may be exceeded especially in the case of hydrogen combustion with oxyfuel. Finally, in case of air combustion flue gas at atmospheric pressure, this model does not account for the decreased line broadening, as it is calibrated on the higher CO2 and H2O partial pressures of oxyfuel conditions. In conclusion, while the model of Bordbar et al. is very flexible and is intended to cover all possible mixture compositions, a model that is closer tailored to the desired conditions is expected to yield improved accuracy. Moreover, the derivation of model coefficients from full spectrum k-distributions is expected to further improve the performance in non-homogeneous cases.

In this paper, a WSGG model is derived for the conditions indicated in Fig. 1. To support its applicability to non-homogeneous cases, the gray gases are derived from full spectrum k-distributions, such that each gray gas represents the same wavenumbers at any gas state. In contrast to a conventional full spectrum k-distribution model, the distributions are evaluated at only 5 quadrature points, in order to maintain the computational expense of a WSGG model. The model is formulated on molar ratio as a variable in the range of $1 \le Mr \le \infty$. Two sets of coefficients are calibrated, one set covering CO_2 and H_2O partial pressures experienced in air combustion flue gas at atmospheric pressure, and

one set calibrated at oxyfuel combustion, respectively. Accuracy of the models is investigated by comparison of total emissivity and predictions for radiative heat flux and volumetric source in a 1D slab. In both cases, benchmarks are obtained from line-by-line integrations.

2. Methodology

The coefficients for the two WSGG models are determined following the same three-step methodology:

- Line-by-line absorption coefficient spectra are computed at discrete temperatures and gas compositions.
- WSGG model weights and absorption coefficients are determined from k-distributions.
- Base functions are fitted to recover the WSGG model weights and absorption coefficients within the calibration range in a continuous manner.

The difference between the models for air and oxyfuel conditions lies in the underlying line-by-line database. In case of oxyfuel combustion, partial pressures of the participating species are increased. While the increase has a minor effect on the $\rm CO_2$ line shape, the $\rm H_2O$ lines are significantly broadened. Since the formulation of the WSGG model does not account for this effect, line-by-line spectra are computed at air and oxyfuel conditions and one set of coefficients is calibrated on each.

2.1. Line by line spectra

For each gas state, absorption spectra are computed line-by-line. In most engineering applications, spectral lines are broadened primarily by molecular collisions, which is described by Lorentz-shaped absorption line profiles [34]. The spectral absorption coefficient κ_{η} at wavenumber η is then obtained from summation over contributions of neighboring spectral lines as

$$\kappa_{\eta} = \sum_{i} \frac{S_{i}}{\pi} \frac{\gamma_{i}}{\gamma_{i}^{2} + (\eta - \eta_{i})^{2}} \tag{1}$$

where S_i is the absorption line intensity of absorption line i. γ_i is the spectral line broadening resulting from air and self broadening:

$$\gamma_i = \left(\frac{T_{\text{ref}}}{T}\right)^n \left[(p_{\text{t}} - p_s) \gamma_{\text{air}} + p_s \gamma_{\text{self}} \right]$$
 (2)

depending on temperature T with temperature dependence coefficient n, total pressure p_t and and partial pressure p_s of species s. Each spectral line is evaluated up to a certain number of Lorentz half-width $n_{\rm Lor}$, given by the generalized cutoff criteria, which Alberti et al. derived for CO_2 [35] and H_2O [36] as a function of temperature and total pressure:

$$n_{\text{Lor,CO2}} = 429.99 \cdot (T/296 \,\text{K})^{0.822} \cdot (1 \,\text{bar}/p_t)^{0.822}$$
 (3)

$$n_{\text{Lor,H2O}} = 686.65 \cdot (T/296 \,\text{K})^{0.833} \cdot (1 \,\text{bar}/p_{\text{t}})^{0.833}$$
 (4)

The line parameters are taken from the high temperature molecular spectroscopic database HITEMP 2010 [3,37], which lists 111×10^6 lines for H_2O and 11×10^6 lines for CO_2 . Spectra are evaluated in the range of $0 < \eta \le 30000$ cm⁻¹ with a resolution of $\Delta \eta = 0.01$ cm⁻¹. Contributions of each line are considered down to an absorption coefficient threshold of 10^{-9} cm⁻¹ or the cutoff halfwidth, whichever yields the narrower interval.

Spectra are calculated for the gas states given in Table 2. Temperature ranges from 300 K to 2700 K for air combustion and up to 3000 K for oxyfuel combustion, covering applications from ambient temperature to the adiabatic flame temperature. Temperatures are varied in steps of $\Delta T = 100$ K. The flue gas compositions treated by the new models include cases where no CO₂, but only H₂O is present. In this case, the standard definition of the molar ratio Mr approaches infinity, and is not suited as a variable for model formulation. Hence, the reciprocal is used in this work, to characterize the CO₂-H₂O mixtures. For the

Table 2
Conditions of line-by-line spectra for WSGG model calibration.

Quantity	Unit	Range	Number of points	Spacing				
Air combustion								
T	K	300-2700	25	Linear				
1/Mr	-	$0 \rightarrow 1$	15	Geometric				
$p_{\mathrm{H2O+CO2}}$	atm	$0.347 \rightarrow 0.262$	15	-				
Oxyfuel combustion								
T	K	300-3000	28	Linear				
1/Mr	-	$0 \rightarrow 1$	15	Geometric				
$p_{\mathrm{H2O+CO2}}$	atm	1	-	-				

range of fuel mixtures considered, the flue gas molar ratio 1/Mr ranges from 0 for pure $\rm H_2O$ to 1 for an equimolar mixture of $\rm CO_2$ and $\rm H_2O$. As total emissivity is sensitive to even small $\rm CO_2$ concentrations, line-by-line evaluations are placed denser in the range where $p_{\rm H2O} \gg p_{\rm CO2}$. The spacing is determined from a geometric sequence of $p_{\rm CO2}$, with $p_{\rm H2O}$ set accordingly, to obtain the compositions given in Fig. 1. The discrete values of molar ratio correspond to the evaluations in Section 3 and may be taken from Figs. 4, 7, and 8. A total of 375 spectra where calculated for air combustion conditions and 420 for oxyfuel conditions.

2.2. Full spectrum k-distribution model

The RTE for an absorbing, emitting, and non-scattering medium is given by [38]

$$\frac{\mathrm{d}I_{\eta}}{\mathrm{d}s} = \kappa_{\eta} I_{\mathrm{b}\eta}(T) - \kappa_{\eta} I_{\eta},\tag{5}$$

with radiative intensity I_{η} at wavenumber η , position s, and spectral Planck function $I_{b\eta}$ at temperature T. In the full spectrum k-distribution (FSK) approach for homogeneous media developed by Modest and Zhang [39] the absorption coefficient is reordered by introduction of a Planck function weighted k-distribution as

$$f(T,k) = \frac{1}{I_b(T)} \int_0^\infty I_{b\eta}(T)\delta(k - \kappa_{\eta}) d\eta$$
 (6)

with black body intensity $I_{\rm b}$, a nominal absorption coefficient k, and the Dirac delta function $\delta(\cdot)$. From multiplication of the RTE in Eq. (5) by the Dirac delta function $\delta\left(k-\kappa_{\eta}\right)$ and integration over the entire spectrum, the RTE for the nominal absorption coefficient reads

$$\frac{\mathrm{d}I_k}{\mathrm{d}s} = kf(T, k)I_\mathrm{b}(T) - kI_k \tag{7}$$

where f denotes the k-distribution and I_k is the intensity per $\mathrm{d}k$ integrated over all spectral locations where $k=\kappa_\eta$. To obtain a smoother distribution, which is better behaved for numerical integration, the cumulative k-distribution g is introduced as

$$g(T,k) = \int_0^k f(T,k) dk$$
 (8)

and yet the RTE is rewritten in terms of g:

$$\frac{\mathrm{d}I_{\mathrm{g}}}{\mathrm{d}s} = kI_{\mathrm{b}}(T) - kI_{\mathrm{g}}.\tag{9}$$

The total intensity employing the different expressions is evaluated from

$$I = \int_0^\infty I_\eta \mathrm{d}\eta = \int_0^\infty I_k \mathrm{d}k = \int_0^1 I_g \mathrm{d}g \tag{10}$$

and the numerical quadrature for evaluation of the integral in g-space now requires relatively few evaluations compared to the expressions over η or k.

2.3. Full spectrum correlated k-distribution model

In the original paper, the FSK approach was extended to non-homogeneous media on the basis of the assumption of a correlated absorption coefficient, and was thus termed the full spectrum correlated k-distribution (FSCK) approach [39]. The absorption coefficient is considered correlated, when at each wavenumber where the absorption coefficient has the same value $k=\kappa_\eta$ at an arbitrary reference gas state, for any other gas state the absorption coefficient at these wavenumbers also has one unique (but possibly different) value. Moreover, the correlated absorption coefficient k^* is required to monotonically increase with k [40]. Although these assumptions are violated by the line-by-line spectra presented in Section 2.1, especially in hot conditions, they are reasonable and are required for the rigorous derivation of the model.

As the properties of the medium may now vary within the domain, they are introduced in the cumulative k-distribution. The gas state is denoted by vector ϕ , which contains the temperature and species partial pressures. The cumulative k-distributions of k at reference state ϕ_0 and of k^* at local state ϕ are related as

$$g(T_{\rm P}, \phi_0, k) = \int_0^k f(T_{\rm P}, \phi_0, k) dk = \int_0^{k^*} f(T_{\rm P}, \phi, k^*) dk^* = g(T_{\rm P}, \phi, k^*)$$
(11)

with T_P indicating the Planck function temperature, not the temperature of the gas. For equal Planck function temperature the same value of g is found for the reference gas state at k and for the local state at k*. Using the correlated absorption coefficient, the RTE is expressed in g_0 -space as

$$\frac{\mathrm{d}I_g}{\mathrm{d}s} = k^*(\phi, k(g_0)) \left[a(T, T_0, g_0) I_b(T) - I_g \right]$$
 (12)

with the scaling function a defined as

$$a(T,T_0,g) = \frac{f(T,\phi_0,k)}{f(T_0,\phi_0,k)} = \frac{\mathrm{d}g(T,\phi_0,k)}{\mathrm{d}g(T_0,\phi_0,k)} = \frac{\mathrm{d}g(T,\phi,k^*)}{\mathrm{d}g(T_0,\phi,k^*)}. \tag{13}$$

The total intensity is obtained from evaluation of the integral from Eq. (10) in g_0 -space using a numerical quadrature scheme

$$I = \sum_{i=1}^{N} w_i I_{g,i} \tag{14}$$

with N evaluations and corresponding weights w_i . As Eq. (14) suggests, the FSCK model is closely related to the WSGG model, which is effectively a low order implementation of the FSCK [39].

A detailed discussion of the relationship between the FSCK and the Spectral Line Weighted Sum of Gray Gases model (SLW) [41,42] is given by Wang et al. [40], stating that the SLW method in the exact limit is equivalent to the FSCK method. Furthermore, the authors provide an overview of the different schemes to determine the correlated absorption coefficients k^* and the scaling function or the gray gas weights, respectively, from k-distributions. In the present model, the methodology termed FSCK2/SLW2 is followed for two reasons: first, the method preserves emission, which is an important performance criterion. Second, the gray gas weights are independent of gas composition and hence, the complexity and number of required model coefficients are limited. For each local state given in Table 2, weights and absorption coefficients are determined from three k-distributions:

- 1. The reference k-distribution with Planck distribution at reference temperature $T_{\rm P}=T_0$, and absorption coefficient evaluated at reference temperature and reference gas composition $\phi=\phi(T_0,x_0)$.
- 2. The *k*-distribution with local state Planck temperature $T_P = T$, and absorption coefficient evaluated at reference conditions $\phi = \phi(T_0, x_0)$.
- 3. The *k*-distribution with with local state Planck temperature $T_{\rm P} = T$, and absorption coefficient evaluated at local conditions $\phi = \phi(T,x)$.

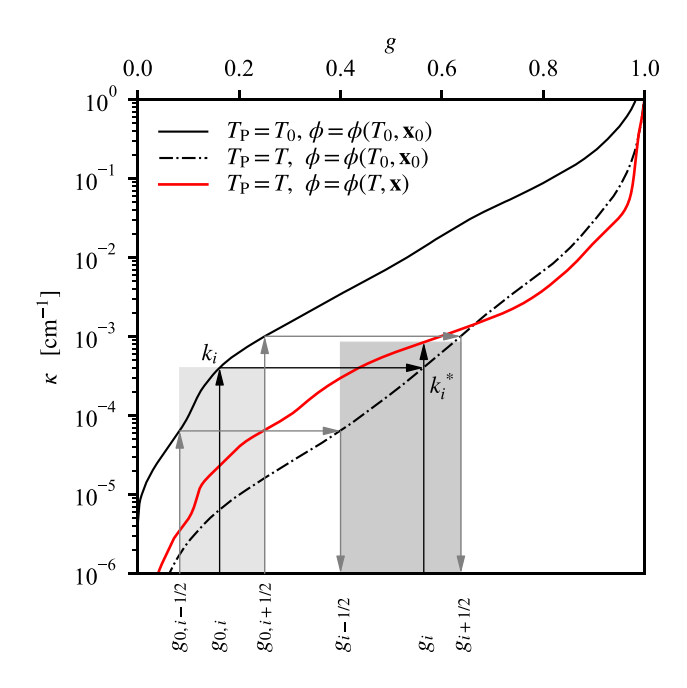


Fig. 2. *k*-distributions of H₂O-CO₂-mixtures at oxyfuel model conditions with reference state $T_0=700\,\mathrm{K},~p_{\mathrm{H2O},0}=0.982\,\mathrm{atm},~p_{\mathrm{CO2},0}=0.018\,\mathrm{atm}$ and local state $T=2500\,\mathrm{K},~p_{\mathrm{H2O}}=1\,\mathrm{atm},~p_{\mathrm{CO2}}=0\,\mathrm{atm}.$

The k-distributions for the reference state and an example local state of the oxyfuel model are given in Fig. 2, together with the scheme to determine gray gas weights and absorption coefficients. The reference k-distribution is discretized using Gaussian quadrature rules with evaluations at $N_{\rm gray}=5$ locations. A quadrature transformation as suggested by Wang et al. [43] is not employed, as it does not improve emissivity predictions at the considered conditions. The value of $g_{0,i}$ and $\Delta g_{0,i} = g_{0,i+1/2} - g_{0,i-1/2}$ are given by the Gaussian sample points and weights. k_i is found from the reference k-distribution at $g = g_{0,i}$. The local g_i is determined from the second k-distribution with local state Planck temperature and reference state absorption coefficient by evaluation at $k = k_i$. In the same manner, the absorption coefficients found in the reference k-distribution at $g_{0,i-1/2}$ and $g_{0,i+1/2}$ are used to determine $g_{i-1/2}$ and $g_{i+1/2}$ in the second k-distribution, with $\Delta g_i = g_{i+1/2} - g_{i-1/2}$. The correlated absorption coefficient for the local state k_i^* is found at $g = g_i$ in the k-distribution with local state Planck temperature and local state absorption coefficient.

While the reference state may be chosen arbitrarily, it is found to influence the performance of the present model. The choice of the reference state is assessed by comparison of total emissivity predictions with the line-by-line integrations. Emissivity is calculated at each calibration database condition at 20 different optical path lengths from 0.01 m to 60 m. The state is then chosen to yield the least relative root mean squared error (RMSE). For the oxyfuel model, the reference state is $T_{0,\rm oxy} = 700\,{\rm K},~p_{\rm H2O,0,oxy} = 0.982\,{\rm atm},~$ and $p_{\rm CO2,0,oxy} = 0.018\,{\rm atm},~$ for the air combustion model, the reference state is $T_{0,\rm air} = 700\,{\rm K},~p_{\rm H2O,0,air} = 0.347\,{\rm atm},~$ and $p_{\rm CO2,0,air} = 0.0\,{\rm atm}.$

2.4. Weighted sum of gray gases model

In the WSGG model the RTE of the *i*th gray gas is expressed as [38]

$$\frac{\mathrm{d}I_i}{\mathrm{d}s} = A_i K_i I_{\mathrm{b}}(T) - K_i I_i \tag{15}$$

with intensity I_i , gray gas weight A_i , and gray gas absorption coefficient K_i , which is related to the pressure absorption coefficient $K_{p,i}$

and the participating species partial pressure p_a as $K_i = p_a K_{p,i}$. The ith absorption coefficient of the WSGG model is then equal to the ith absorption coefficient of the FSCK model and the WSGG weights relate to the FSCK scaling function and quadrature weight as

$$A_i = a_i w_i. (16)$$

To obtain a continuous representation of A_i and $K_{p,i}$ within the calibration range of the air and oxyfuel model in terms of temperature and composition, base functions are fitted to recover the weights and absorption coefficients that are derived from the k-distributions. Using the FSCK2 scheme, weights A_i are independent of the local gas composition and vary only with temperature. In the present model, the polynomial is built on the natural logarithm of the gas temperature, which is found to allow for a more accurate fit compared to a polynomial built on a normalized temperature, as many authors suggest, especially at temperatures $T < 1000 \, \text{K}$. The weights are then calculated from coefficients $b_{i,k}$ as

$$A_i = \sum_{k=0}^{4} b_{i,k} \ln \left(\frac{T}{1 \,\mathrm{K}}\right)^k. \tag{17}$$

Absorption coefficients on the other hand are determined at local gas temperature and composition, consequently depending on both. Therefore, in addition to temperature, the polynomial formulation incorporates the molar ratio. Pressure absorption coefficients are calculated from coefficients $c_{i,i,k}$ as

$$K_{p,i} = \sum_{k=0}^{4} \sum_{j=0}^{4} c_{i,j,k} (1/Mr)^{m_{j+1}} \ln\left(\frac{T}{1 \text{ K}}\right)^{k}, \quad \mathbf{m} = [0, 0.25, 0.5, 1, 2]$$
 (18)

with molar ratio exponents given by vector m. The calibrated model coefficients $b_{i,k}$ and $c_{i,j,k}$ are given in Tables A.5 and A.6. Model implementations in Python [44] and as user defined functions for Ansys Fluent [45] are provided as supplementary material.

3. Results

The performance of the WSGG models calibrated for air combustion and oxyfuel combustion is evaluated by comparison of total emissivity predictions and predictions for radiative heat flux and source term in a 1D slab.

3.1. Total emissivity

Total emissivity along a path is a measure for the radiative intensity originating from the gas due to emission and self absorption. WSGG model predictions of total emissivity are used for instance in commercial CFD software as Ansys Fluent [45], to deduce a single gray gas absorption coefficient that recovers the emissivity for a characteristic path length. The RTE is then solved for this single gray gas, rather then for each of the weighted gray gases. Further, it is established practice to assess the accuracy of WSGG models by comparison of total emissivity to higher order models such as line-by-line integrations. Total emissivity ε of a gas column at path length L is evaluated from the WSGG model as

$$\varepsilon_{\text{wsgg}} = \sum_{i=1}^{N} A_i [1 - \exp(-K_{p,i} p_a L)]. \tag{19}$$

The benchmark emissivity is calculated from line-by-line integration as

$$\varepsilon_{\text{lbl}} = \frac{1}{\sigma T^4} \sum_{i=1}^{N_{\eta}} E_{b\eta j} \left[1 - \exp\left(-\kappa_j L \right) \right]$$
 (20)

under the assumptions and discretisation given in Section 2.1. σ is the Stefan–Boltzmann constant, $E_{b\eta j}$ is the Planck function at wavenumber η_j and interval $\Delta\eta$, κ_j is the absorption coefficient at η_j . Total emissivity is evaluated at all conditions for air and oxyfuel combustion flue gas

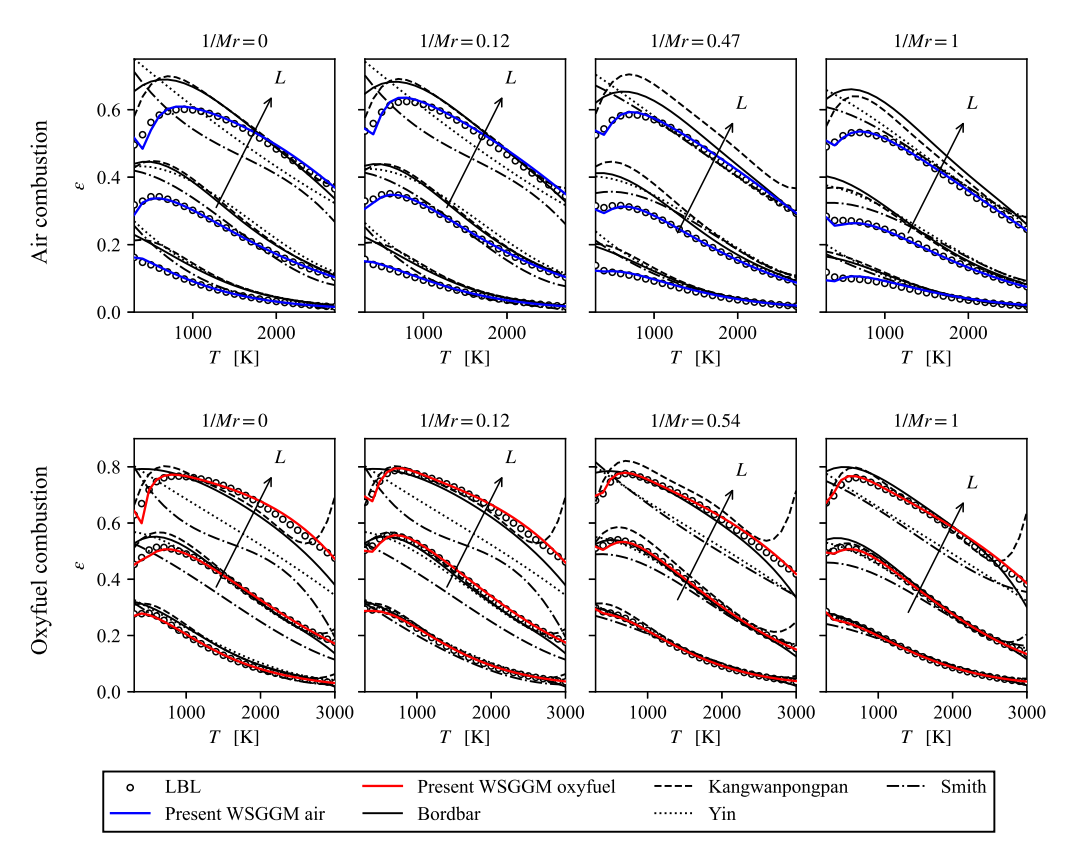


Fig. 3. Emissivity of the proposed WSGG model over temperature in comparison to line-by-line integration and other WSGG models at partial pressures representative for air and oxyfuel combustion and path length $L \in [0.1, 1, 10]$ in m.

 Table 3

 Total emissivity prediction RMSE of WSGG models evaluated at path length of 0.01, 0.05, 0.1, 0.2, 0.3, 0.4, 0.5, 0.75, 1, 1.5, 2, 3, 5, 10, 15, 20, 30, 40, 50, and 60 m.

Model	Error				
	Air combustion	Oxyfuel combustion			
Smith et al.	0.0870	0.1565			
Yin et al.	0.0671	0.0836			
Kangwanpongpan et al.	0.0544	0.0578			
Bordbar et al.	0.0546	0.0373			
Present WSGGM	0.0105	0.0277			

provided in Section 2.1 and Table 2 in particular. Predictions are compared against the WSGG models of Smith et al. [46], as it still today is widely used in commercial CFD software [45], Yin et al. [13], Kangwanpongpan et al. [16], and Bordbar et al. [24], as these models are in the closest agreement with the evaluated molar ratios. Emissivity is evaluated at 0.1, 1, and 10 m path length.

Results of emissivity at varying temperature are given in Fig. 3 for different molar ratios. The compositions may be interpreted from left to right as flue gas compositions of combustion of hydrogen, a blend of hydrogen and methane, methane, and octane or biogas with 50% CO2 content (see Fig. 1). Partial pressures of H2O and CO2 are lower at air combustion conditions, yielding lower emissivity at equal molar ratio and path length. The models of Kangwanpongpan and Bordbar are calibrated for temperatures down to 400 K and 300 K and correctly suggest a peak of emissivity at temperatures below 1000 K for path length of 1 m and 10 m. The model of Kangwanpongpan shows a more accurate prediction of decreasing emissivity towards lower temperatures than the model of Bordbar. The behavior of the latter is in agreement with its underlying line-by-line data. Deviations to the present line-by-line emissivities may be due to the details of spectra computation, as the present study follows the cut-off criteria suggested by Alberti et al. [35,36]. The models of Smith and Yin are calibrated

for temperatures down to 600 K and 500 K and fail to predict this trend. For air combustion conditions, an overprediction of emissivity by the models from literature is observed at path length of 0.1 and 1 m and is particularly pronounced at lower temperature. This behavior is expected for the models of Yin, Kangwanpongpan, and Bordbar, since these authors calibrated their models at oxyfuel conditions at atmospheric pressure. The self broadening of H₂O in conjunction with the higher H₂O partial pressures compared to air combustion causes an overprediction of total emissivity. Consequently, in case of oxyfuel combustion, no such general trend is observed. At these conditions, higher temperatures may be expected and the evaluation is performed up to 3000 K. Only the model of Yin et al. is calibrated up to this temperature. However, at 10 m path length it underpredicts emissivity at temperatures $T > 500 \,\mathrm{K}$ for each of the evaluated compositions. The model of Kangwanpongpan et al. is calibrated up to 2500 K. Overprediction of emissivity at higher temperature is observed particularly at the longer path length and suggests, that the model should not be used at temperatures exceeding this limit. The new models provide the most accurate predictions of total emissivity and closely follow the line-by-line integrated emissivity in the whole range of temperature, compositions, and path length.

Total emissivity varying with molar ratio is given in Fig. 4 at different temperatures for air and oxyfuel combustion conditions. The markers of line-by-line integrations indicate the denser spacing of evaluations closer to 1/Mr=0. It is observed at these lower CO_2 contents, that emissivity decreases towards the condition, where only H_2O and no CO_2 is present. This behavior is not properly captured by current WSGG models. The dependency of emissivity prediction on molar ratio is isolated in the plots at oxyfuel conditions, since partial pressure of the participating gases $p_a=1$ atm and temperature are constant in this evaluation. Hence, variations of emissivity are only attributed to varying molar ratio. The model of Smith provides coefficients for pure water, 1/Mr=0.5, and 1/Mr=1, while it is up to the user to

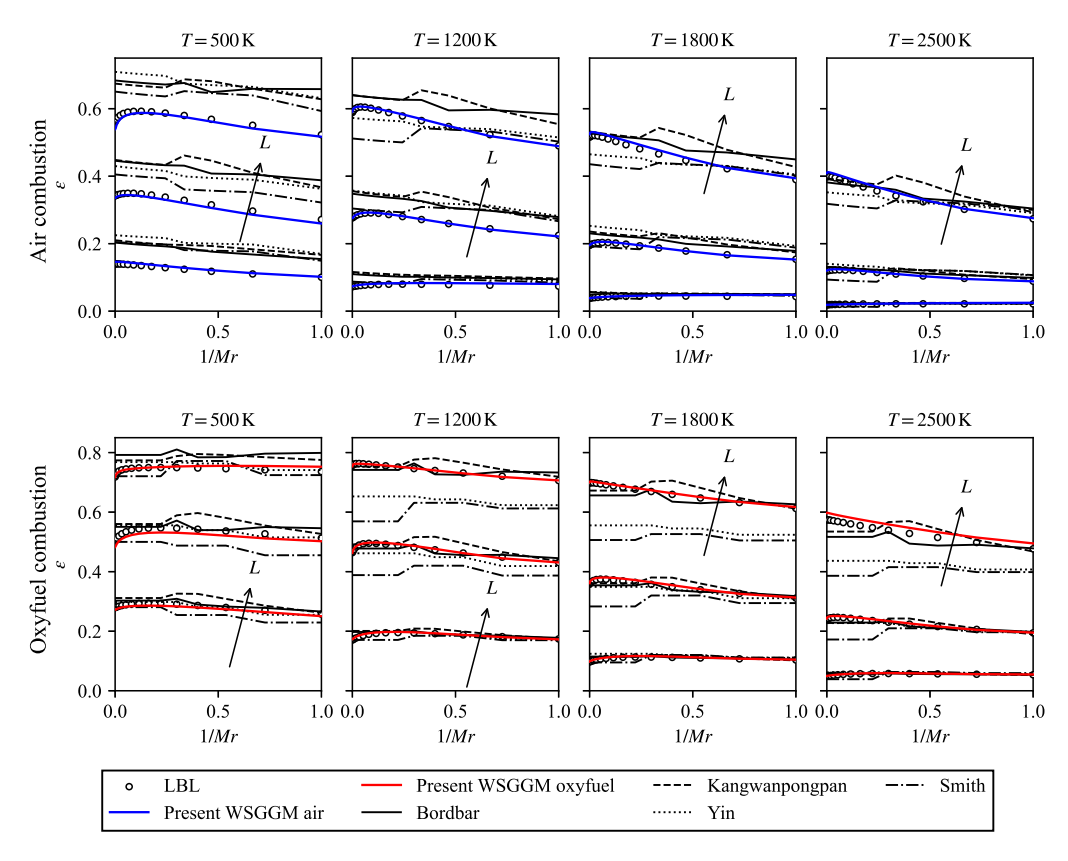


Fig. 4. Emissivity of the proposed WSGG model over molar ratio in comparison to line-by-line integration and other WSGG models at partial pressures representative for air and oxyfuel combustion and path length $L \in [0.1, 1, 10]$ in m.

decide on the range of molar ratio at which the respective coefficients are applied. In this study, coefficients are changed at molar ratios 1/Mr = 0.25, and 1/Mr = 0.667. This procedure appears as jumps in the emissivity when transitioning between different ranges. The models of Yin et al. and Kangwanpongpan et al. are calibrated up to a molar ratio of 1/Mr = 0.25. The prediction of this molar ratio is simply used for any molar ratio in the evaluation that is beyond this limit and hence, is constant for the oxyfuel cases. Bordbar et al. extend the validity of their model beyond 1/Mr = 0.25 by adding a coefficient calibration for $1/Mr = 10^{-8}$ and computing the coefficients for intermediate values of Mr by interpolation. However, the suggested scheme yields emissivity predictions that appear constant over a wide range of molar ratio and experience an abrupt decrease at $1/Mr \rightarrow 0$, which is not observed in the line-by-line integrations.

The root mean squared errors (RMSE) of WSGG total emissivity predictions compared to the line-by-line results at all temperatures and compositions considered for the calibration are given in Table 3. Evaluations are performed at 20 different path length between 1 cm and 60 m. For air and oxyfuel combustion scenarios, the model of Smith et al. yields the largest errors, as it is the simplest model in the comparison with the fewest gray gases and reference compositions. It is noticed, that the more recent and the more elaborate the models are, the smaller the errors. Despite for the model of Bordbar, errors are higher for oxyfuel combustion than for air combustion, even though the models of Yin and Kangwanpongpan are calibrated at oxyfuel conditions. This tendency may be explained by the fact that errors are not normalized in this evaluation and higher total emissivities are experienced under oxyfuel conditions. Moreover, the evaluation at oxyfuel conditions covers higher temperatures of up to 3000 K, which is beyond the calibrated range of several models and hence, unfavourable for their performance. The models for air and oxyfuel combustion proposed in this study provide the most accurate predictions of total emissivity. The dependencies on temperature and molar ratio are well

captured, especially at low temperatures, and at mixture compositions with minor CO2 contents, the new models recover the line-by-line benchmark significantly more accurate compared to the WSGG models from literature. The ability to follow these dependencies is attributed to the choice of base functions, i.e. the polynomials based on temperature logarithm and the inverse of molar ratio.

3.2. 1D slab

It is established practice to assess the performance of WSGG models in a one-dimensional slab, consisting of a participating gas in between two infinite parallel plates [20-27]. The plates are black and are separated by distance S. Employing the discrete ordinates method (DOM), the problem is discretised into a finite number of directions. The RTEs for gray gas i along direction l in forward and backward direction are

$$\mu_{l} \frac{\mathrm{d}I_{i,l}^{+}(s)}{\frac{\mathrm{d}s}{\mathrm{d}s}} = -K_{p,i} p_{a} I_{i,l}^{+}(s) + K_{p,i} p_{a} A_{i} I_{b}$$

$$\frac{\mathrm{d}I_{-}^{-}(s)}{\mathrm{d}s} = -K_{p,i} p_{a} I_{i,l}^{+}(s) + K_{p,i} p_{a} A_{i} I_{b}$$
(21)

$$-\mu_{l} \frac{\mathrm{d}I_{i,l}^{-}(s)}{\mathrm{d}s} = -K_{p,i}p_{a}I_{i,l}^{-}(s) + K_{p,i}p_{a}A_{i}I_{b}$$
 (22)

with the forward and backward intensities $I_{i,l}^+(s)$ and $I_{i,l}^-(s)$, and the cosine in direction l denoted by μ_l . Boundary conditions at the black walls are given as $I_{i,l}^+(s=0) = A_i I_b|_{s=0}$ at the left, and $I_{i,l}^-(s=S) = A_i I_b|_{s=S}$ at the right wall. The equations are solved using an implicit stepping scheme. The radiative heat flux $q_r''(s)$ and the radiative source term to the energy equation $\dot{q}_r(s)$ are computed according to

$$q_r''(s) = \sum_{i=0}^{I} \sum_{l=0}^{L} 2\pi \mu_l w_l \left(I_{i,l}^+(s) - I_{i,l}^-(s) \right)$$

$$\dot{q}_r(s) = \sum_{i=0}^{I} \sum_{l=0}^{L} 2\pi w_l K_{p,i} p_a(s) \left[\left(I_{i,l}^+(s) - I_{i,l}^-(s) \right) - 2A_i(s) I_b(s) \right]$$
(23)

$$\dot{q}_r(s) = \sum_{i=0}^{I} \sum_{l=0}^{L} 2\pi w_l K_{p,i} p_a(s) \left[\left(I_{i,l}^+(s) - I_{i,l}^-(s) \right) - 2A_i(s) I_b(s) \right]$$
 (24)

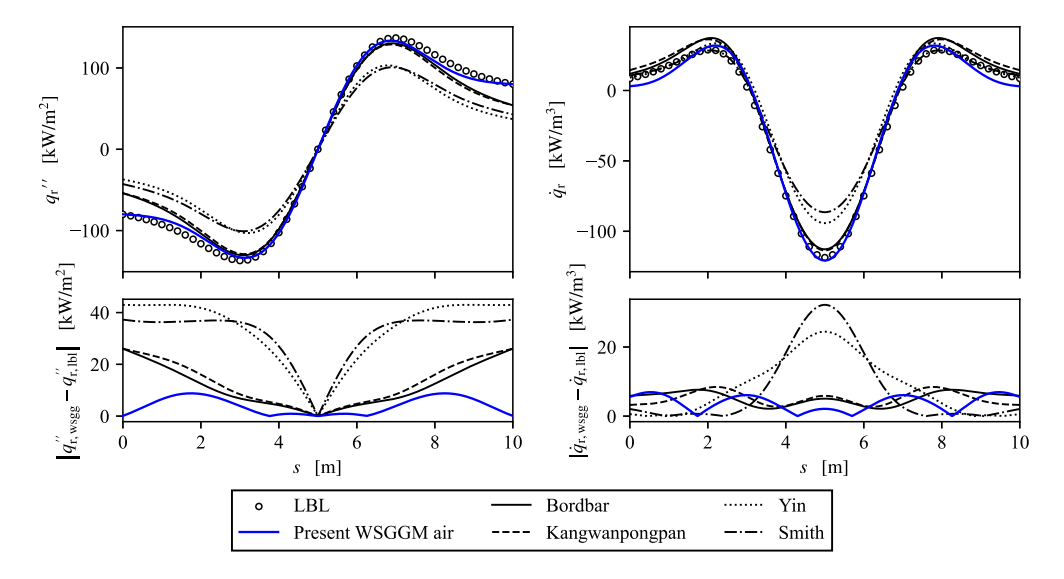


Fig. 5. Radiative heat flux q_r'' and radiative source term \dot{q}_r of case 2.6 with temperature distribution $T(\hat{s}) = 400 + 1400 \sin^2(\pi \hat{s})$, $p_{\rm H2O} = 0.325$ atm, and $p_{\rm CO2} = 0.013$ atm.

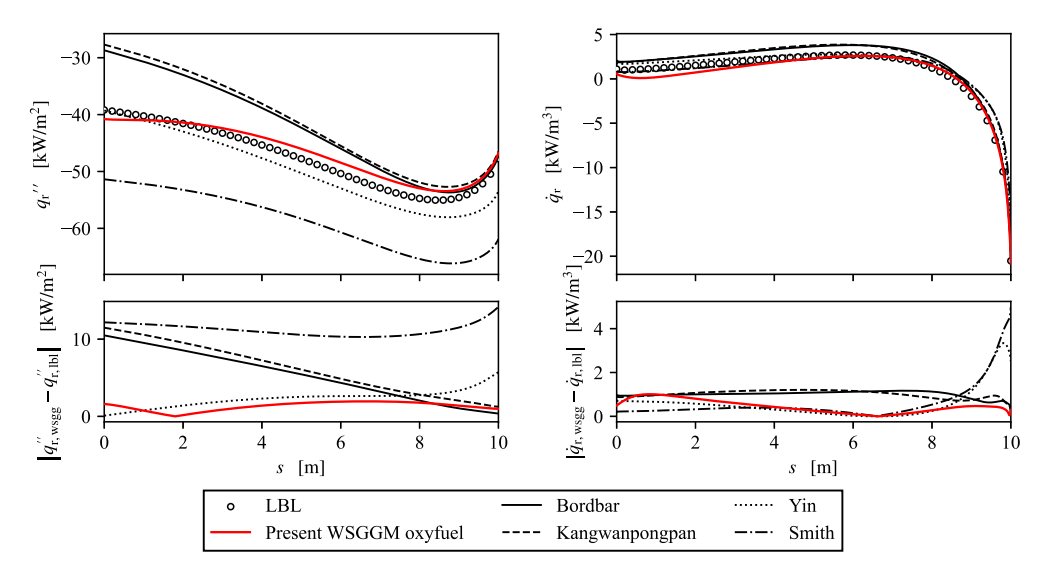


Fig. 6. Radiative heat flux $q_r^{\prime\prime}$ and radiative source term \dot{q}_r of case 8.6 with temperature distribution $T(\hat{s}) = 300 + 900\hat{s}$, $p_{\rm H2O} = 0.950$ atm, and $p_{\rm CO2} = 0.050$ atm.

with w_l denoting the quadrature weight of direction l. The domain is discretized into 500 equidistant spatial elements and the S8 scheme is used for angular discretization [34]. The problem is solved at homogeneous gas compositions within the domain for every composition from the calibration database. The definitions of all cases are given in Table 4. Two temperature distributions are imposed on the domain. The first distribution is symmetric with a peak temperature of 1800 K at the center and walls at 400 K. The second distribution is increasing linearly with distance from 300 K at the left wall to 1200 K at the right wall. The length of the domain is set to either 1 m or 10 m. The variations of composition, temperature distribution, and domain size yield a total of 120 cases. The comparison involves the same WSGG models as in Section 3.1. The benchmark solution is provided by lineby-line integration. The RTE given in Eq. (21) and (22) is then solved accordingly not for gray gas i, but rather for wavenumber interval i. As line-by-line spectra are computed and tabulated at temperatures in steps of $\Delta T = 100 \,\mathrm{K}$, spectra at intermediate temperatures are obtained from interpolation using cubic splines.

As an example of cases with hot gas between cold walls, the radiative heat flux and source term for case 2.6 are shown in Fig. 5, along with the errors in respect to the line-by-line benchmark. The magnitude of radiative heat flux is underpredicted in the entire domain by the

Table 4 One dimensional slab cases with dimensionless distance $\hat{s} = s/S$.

Case	T [K]	$T[K]$ $p_{H2O+CO2}[atm]$		S [m]				
Air combustion	l							
1.1 to 1.15	$400 + 1400 \sin^2(\pi \hat{s})$	$0.347 \rightarrow 0.262$	$0 \rightarrow 1$	1				
2.1 to 2.15	$400 + 1400 \sin^2(\pi \hat{s})$	$0.347 \rightarrow 0.262$	$0 \rightarrow 1$	10				
3.1 to 3.15	$300 + 900\hat{s}$	$0.347 \rightarrow 0.262$	$0 \rightarrow 1$	1				
4.1 to 4.15	$300 + 900\hat{s}$	$0.347 \rightarrow 0.262$	$0 \rightarrow 1$	10				
Oxyfuel combustion								
5.1 to 5.15	$400 + 1400 \sin^2(\pi \hat{s})$	1.0	$0 \rightarrow 1$	1				
6.1 to 6.15	$400 + 1400 \sin^2(\pi \hat{s})$	1.0	$0 \rightarrow 1$	10				
7.1 to 7.15	$300 + 900\hat{s}$	1.0	$0 \rightarrow 1$	1				
8.1 to 8.15	$300 + 900\hat{s}$	1.0	$0 \rightarrow 1$	10				

models of Smith et al. and Yin et al. The models of Kangwanpongpan et al. and Bordbar et al. yield predictions closer to the benchmark while being less accurate closer to the walls. The proposed model for air combustion yields the prediction with the closest agreement within the entire domain. For the radiative source term, there is no single model that performs best at all locations. While the new model provides the highest accuracy at the high temperatures at the center of the

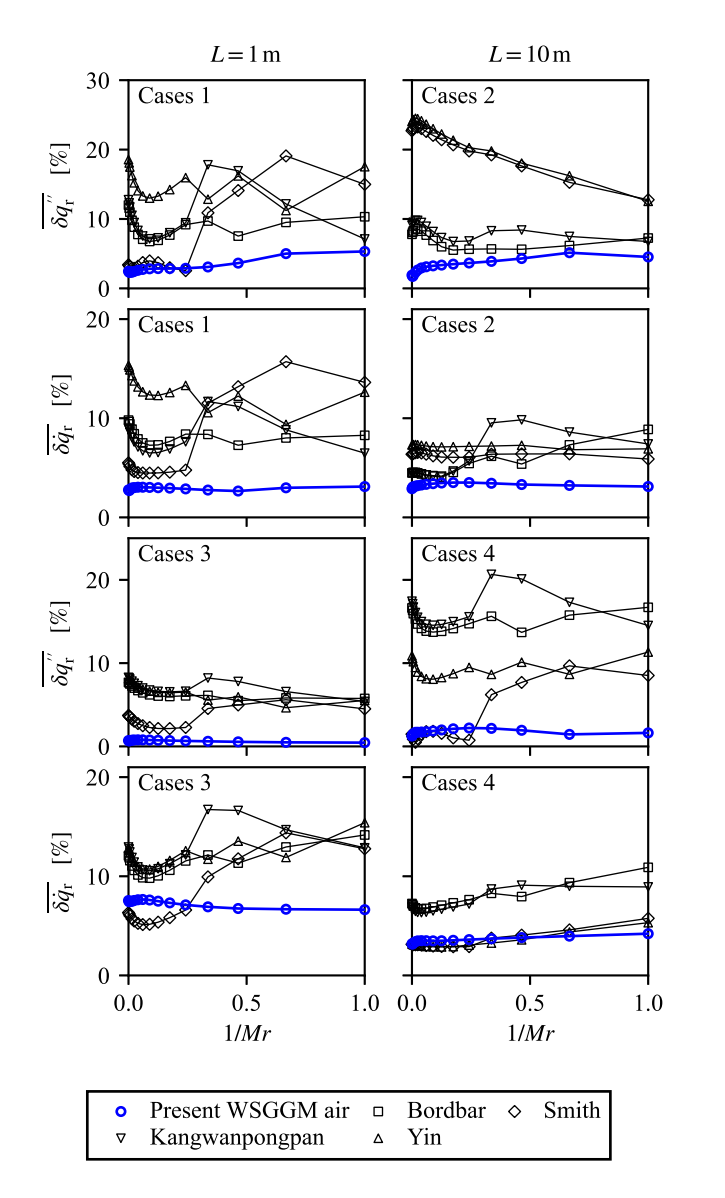


Fig. 7. Averaged, normalized errors of radiative heat flux $\overline{\delta q''_r}$ and source term $\overline{\delta \dot{q}_r}$ at air combustion conditions.

domain, the models of Smith and Yin are in better agreement with the benchmark at lower temperatures in vicinity of the walls.

An example of the cases with a cold and a hot wall is provided in Fig. 6 with radiative heat flux and source term given for case 8.6. The radiative heat flux is recovered closest by the new model. The models of Smith et al. and Yin et al. overpredict the heat flux magnitude within the entire domain. At the cold temperatures close to the left wall, however, the Yin model is in close agreement with the benchmark. At this location, the models of Kangwanpongpan et al. and Bordbar et al. underpredict the heat flux magnitude, while both models yield a more accurate prediction towards the higher temperatures close to the right wall. As it is observed in the error plot of radiative heat flux, the smallest average error is produced by the proposed new model. For the radiative source term the models of Smith and Yin again, yield lower errors towards the left wall and show increasing deviations from the benchmark towards the hot right wall. The models of Kangwanpongpan and Bordbar overpredict the source term at every location within the domain. The new model underpredicts the source term towards the left wall, producing higher errors compared to the models of Smith and Yin.

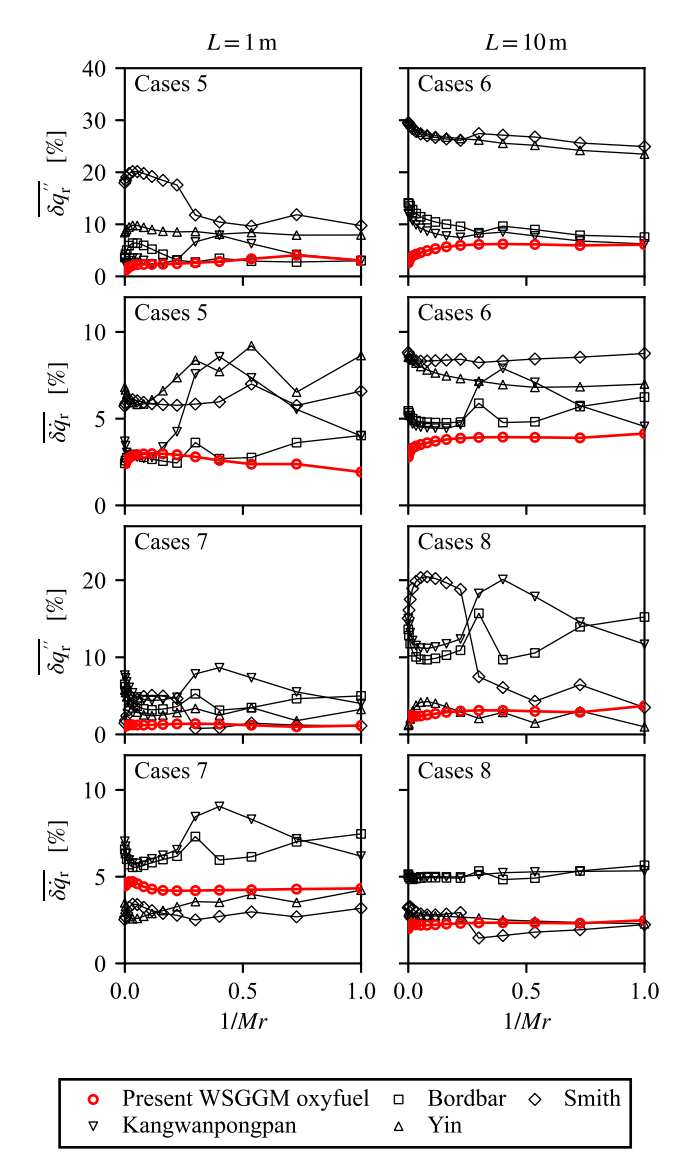


Fig. 8. Averaged, normalized errors of radiative heat flux $\overline{\delta q''_r}$ and source term $\overline{\delta \dot{q}_r}$ at oxyfuel combustion conditions.

Nevertheless, considering the entire domain, the prediction of the new model yields the smallest error in the comparison.

To assess the performance of the models across all evaluated cases listed in Table 4, the errors in radiative heat flux and source term are calculated for each case as follows:

$$\delta q_{\rm r}^{\prime\prime} = \frac{|q_{\rm r,wsgg}^{\prime\prime} - q_{\rm r,lbl}^{\prime\prime}|}{\max|q_{\rm r,lbl}^{\prime\prime}|} \tag{25}$$

$$\delta \dot{q}_{\rm r} = \frac{|\dot{q}_{\rm r,wsgg} - \dot{q}_{\rm r,lbl}|}{\max |\dot{q}_{\rm r,lbl}|}$$
(26)

and averaged over the domain. Cases of air combustion conditions are depicted in Fig. 7 and oxyfuel conditions in Fig. 8. The subplots in each figure are arranged as follows: in the upper left, errors of radiative heat flux for the case of hot gas between cold walls are given, source term errors of the same case are provided in the subplot below. This case represents a domain size of 1 m. The corresponding plots in the right column show the next case, which is equivalent to the previous, despite a larger domain size of 10 m. The next four subplots follow the same arrangement, but for the cases of a cold and a hot wall. Within

each subplot, the average errors are shown depending on molar ratio, representing all considered compositions in sub cases X.1 to X.15 in each case X.

For cases 1 the new model predicts the heat flux with less then 6% averaged error and source term with less then 4% averaged error at every considered composition. The compared models yield considerably higher errors, despite the model of Smith et al. at the cases for molar ratio close to 1/Mr = 0. For cases 2, where the domain is extended to 10 m in length, the models of Bordbar and Kangwanpongpan provide heat flux predictions with errors between 5% and 10%, while the errors of models from Yin and Smith even exceed 20% for 1/Mr < 0.2. Again, heat flux predictions of the new model yield errors below 6% and heat source predictions are below 4% averaged errors at all compositions. For the cases 3 and 4, where the medium is bounded between a cold and a hot plate, the new model yields the most accurate heat flux predictions compared to the literature models, not exceeding errors of 1% at the 1 m domain, and 3% at the 10 m domain at any composition. Only the predictions of Smith at 1/Mr < 0.3 at case 4 show comparable or even higher accuracy. Similarly, the heat source predictions of the Smith model in case 3 are the most accurate, while for 1/Mr > 0.3, the new model yields the smallest errors. In case 4, the predictions closest to the benchmark are provided by the new model and the models of

For the oxyfuel cases 5 and 6, where the hot gas is confined between two cold plates, the new model predicts the heat flux and source term with the lowest errors. Only the model of Bordbar shows comparable accuracy and with even lower errors for the source term at conditions of 1/Mr < 0.3 at case 5. The models of Smith and Yin provide the highest errors for the majority of compositions, both yielding a maximum error of over 29% for radiative heat flux in pure $\rm H_2O$ atmosphere of case 6.1. For cases 7 and 8 with a cold and hot wall, the new model predicts the heat flux with errors less than 4% and the source term with errors less than 5%. The only model, that delivers the same order of accuracy for heat flux and source term at these cases is the one from Yin. Each of the other models shows large errors in at least one of the cases. The predictions of heat flux in cases 8 for instance, all reach errors greater than 10% at the majority of compositions.

From evaluation of the 1D slab cases it is concluded, that the new model provides significantly increased accuracy over the models included in the comparison over a wide range of conditions. The new model is proven to be applicable in the desired range of molar ratios. Even while at few conditions, other models yield smaller averaged errors, no single model from literature is found to provide comparable accuracy over such variety of cases. At air combustion conditions in particular, the new model shows the highest overall accuracy for every case.

4. Conclusion

A WSGG model formulation with 5 gray gases was proposed to cover combustion flue gas compositions with molar ratio $Mr = p_{\rm H2O}/p_{\rm CO2}$ in the range of $1 \le Mr \le \infty$ ($0 \le 1/Mr \le 1$). Two sets of coefficients were calibrated to account for the difference in H2O partial pressure at combustion with air and oxyfuel at atmospheric pressure. The models are valid within the temperature range of $300 \,\mathrm{K} \le T \le 2700 \,\mathrm{K}$ for air combustion and $300 \,\mathrm{K} \le T \le 3000 \,\mathrm{K}$ for oxyfuel combustion. The gray gas weights and absorption coefficients were derived from k-distributions obtained from line-by-line computations based on the HITEMP2010 spectroscopic database. The WSGG parameters derived from k-distributions have actual physical significance, as they represent the same spectral intervals at all conditions. Hence, compared to the derivation based on total emissivity fitting, the model is conceptually better suited to describe cases, which are non-homogeneous in terms of temperature and species composition. Base functions were fitted to continuously recover the weights and absorption coefficients within the range of calibration. The accuracy of the model was assessed

by predictions of total emissivity as well as radiative heat flux and source term in a 1D slab. Benchmark solutions were obtained from line-by-line integrations covering all compositions of the WSGG model calibration database. The new model showed significantly improved predictions when compared to WSGG models from literature. It is applicable in a wide range of flue gas compositions resulting from the combustion of hydrogen, methane, octane, biogas, or mixtures of these fuels. The model covers exhaustive temperature ranges from standard ambient temperature up to the adiabatic flame temperature. It should be noted that the species partial pressures in the calibration database are representative of stoichiometric combustion at atmospheric pressure. However, the model might be used under conditions deviating from the calibration database shown in Fig. 1, for instance at higher or lower total pressure, at fuel rich or lean conditions, or at combustion with oxygen-enriched air. In this case, the user is advised to select the model coefficients for air or oxyfuel combustion for which the calibration H₂O partial pressure is in closer agreement with the flue gas conditions, as it is decisive for the non-linear effect of spectral line broadening.

CRediT authorship contribution statement

Johannes Losacker: Writing – original draft, Visualization, Software, Methodology, Investigation, Conceptualization. Alex M. Garcia: Writing – review & editing, Validation, Methodology, Conceptualization. Nico Schmitz: Writing – review & editing, Resources, Project administration, Funding acquisition, Conceptualization. Christian Wuppermann: Writing – review & editing, Resources, Funding acquisition.

Declaration of competing interest

The authors declare the following financial interests/personal relationships which may be considered as potential competing interests: Johannes Losacker reports financial support was provided by European Union. Johannes Losacker reports article publishing charges was provided by German Research Foundation. If there are other authors, they declare that they have no known competing financial interests or personal relationships that could have appeared to influence the work reported in this paper.

Acknowledgments

This work has received funding from the European Union's Horizon Europe research and innovation programme under grant agreement No 101091456.

Appendix. Wsgg model coefficients

See Tables A.5 and A.6.

Data availability

Model implementations in Python and as Ansys Fluent UDFs are available under the shared link.

WSGGM Implementations (Original data) (Git)

Table A.5
Air combustion model coefficients.

Coeff.	Unit	i	j	k = 0	k = 1	k = 2	k = 3	k = 4
b	-	0	-	50.987613	-30.412657	6.785040	-0.673384	0.025245
c	m^{-1} at m^{-1}	0	0	-34.854459	21.228519	-4.825173	0.484898	-0.018169
c	m^{-1} at m^{-1}	0	1	-2.891444	1.749327	-0.394982	0.039434	-0.001468
c	m^{-1} at m^{-1}	0	2	10.352167	-6.262756	1.413944	-0.141147	0.005254
c	m^{-1} at m^{-1}	0	3	19.533138	-11.948951	2.727956	-0.275350	0.010362
c	m^{-1} at m^{-1}	0	4	-8.475105	5.174966	-1.179341	0.118832	-0.004464
b	-	1	-	-32.285675	18.941499	-4.148033	0.404829	-0.014855
c	$m^{-1} atm^{-1}$	1	0	-15.324297	11.713791	-3.205618	0.375638	-0.015968
c	$m^{-1} atm^{-1}$	1	1	-27.238662	17.608427	-4.240228	0.450481	-0.017799
c	m^{-1} at m^{-1}	1	2	429.446894	-257.261735	57.469580	-5.673473	0.208844
c	m^{-1} at m^{-1}	1	3	-526.383114	309.832997	-67.939803	6.578485	-0.237412
c	m^{-1} at m^{-1}	1	4	170.316706	-99.426840	21.609217	-2.072557	0.074048
b	-	2	-	-49.012909	29.175744	-6.483475	0.641678	-0.023886
c	m^{-1} at m^{-1}	2	0	481.974363	-278.442643	59.646693	-5.614026	0.196039
c	m^{-1} at m^{-1}	2	1	-407.096943	245.878350	-55.164541	5.446718	-0.199729
c	m^{-1} at m^{-1}	2	2	2181.092966	-1308.530411	291.602208	-28.598369	1.041815
c	m^{-1} at m^{-1}	2	3	-3163.052023	1882.713653	-416.427238	40.557614	-1.468187
c	m^{-1} at m^{-1}	2	4	1160.344936	-688.339977	151.803136	-14.748963	0.532910
b	_	3	_	-0.429114	0.106180	0.054725	-0.012586	0.000632
c	$m^{-1} atm^{-1}$	3	0	527.393004	-366.041569	90.956184	-9.662186	0.373185
c	m^{-1} at m^{-1}	3	1	-2397.080114	1398.627532	-303.304120	28.966150	-1.028348
c	m^{-1} at m^{-1}	3	2	8203.256650	-4791.900873	1040.308196	-99.447192	3.533448
c	m^{-1} at m^{-1}	3	3	-3511.702460	2135.380970	-480.379439	47.361973	-1.728644
c	m^{-1} at m^{-1}	3	4	-1486.583638	849.462336	-181.614873	17.233000	-0.612278
b	_	4	_	31.740086	-17.810767	3.791743	-0.360537	0.012864
c	m^{-1} at m^{-1}	4	0	-15271.973219	8371.837816	-1699.116384	151.926351	-5.063307
c	m^{-1} at m^{-1}	4	1	-9987.949025	5929.485612	-1310.198370	127.703525	-4.632627
c	m^{-1} at m^{-1}	4	2	40 039.398179	-23935.599448	5327.850616	-523.305223	19.135577
c	m^{-1} at m^{-1}	4	3	51 136.742624	-29165.082513	6168.620407	-573.897030	19.845240
c	$m^{-1} at m^{-1}$	4	4	-27433.700119	16 058.644295	-3497.203943	336.048437	-12.033936

Table A.6Oxyfuel combustion model coefficients.

Coeff.	Unit	i	j	k = 0	k = 1	k = 2	k = 3	k = 4
b	-	0	_	43.856044	-25.869502	5.702038	-0.559329	0.020782
c	m^{-1} at m^{-1}	0	0	-30.065795	18.482879	-4.239654	0.429838	-0.016240
c	m^{-1} at m^{-1}	0	1	-2.607840	1.575883	-0.355191	0.035378	-0.001313
c	m^{-1} at m^{-1}	0	2	9.191146	-5.555119	1.252358	-0.124769	0.004633
c	m^{-1} at m^{-1}	0	3	16.557259	-10.175471	2.333715	-0.236593	0.008939
c	m^{-1} at m^{-1}	0	4	-7.909467	4.816043	-1.094340	0.109929	-0.004117
b	_	1	_	-62.869691	37.276801	-8.237566	0.807324	-0.029613
c	m^{-1} at m^{-1}	1	0	28.505373	-13.284910	2.078391	-0.114837	0.000916
c	m^{-1} at m^{-1}	1	1	53.371129	-29.922543	6.194764	-0.560447	0.018677
c	m^{-1} at m^{-1}	1	2	426.300740	-255.480190	57.087108	-5.636328	0.207457
c	m^{-1} at m^{-1}	1	3	-654.957785	384.492203	-84.068372	8.114823	-0.291874
c	m^{-1} at m^{-1}	1	4	223.896195	-130.612929	28.366537	-2.718606	0.097051
b	-	2	_	-28.453564	16.763303	-3.692504	0.364600	-0.013637
c	m^{-1} at m^{-1}	2	0	783.583250	-455.574244	98.273957	-9.319870	0.328066
c	m^{-1} at m^{-1}	2	1	-706.877092	429.909793	-97.119494	9.655147	-0.356473
c	m^{-1} at m^{-1}	2	2	4061.439632	-2445.196928	546.911430	-53.844254	1.969343
c	m^{-1} at m^{-1}	2	3	-5302.653728	3167.020430	-702.858858	68.680883	-2.494179
c	m^{-1} at m^{-1}	2	4	1712.247594	-1019.159434	225.420450	-21.955475	0.794848
b	-	3	_	10.099800	-6.744518	1.696257	-0.184703	0.007305
c	m^{-1} at m^{-1}	3	0	-656.619351	253.144269	-28.627992	0.469600	0.055020
c	m^{-1} at m^{-1}	3	1	-4754.383357	2800.497778	-614.246009	59.433136	-2.140921
c	m^{-1} at m^{-1}	3	2	16828.414562	-9925.858407	2179.782823	-211.144652	7.613421
c	m^{-1} at m^{-1}	3	3	-11404.316523	6849.093227	-1529.044271	150.318070	-5.492895
c	m^{-1} at m^{-1}	3	4	1626.190923	-987.243471	221.963342	-21.912633	0.802588
b	-	4	_	38.367411	-21.426084	4.531775	-0.427891	0.015163
c	m^{-1} at m^{-1}	4	0	-29253.699889	16 457.434810	-3436.929839	316.647039	-10.878843
c	m^{-1} at m^{-1}	4	1	-385.794720	748.652640	-285.064516	39.940085	-1.906726
c	m^{-1} at m^{-1}	4	2	15 360.090683	-10841.332783	2798.629053	-314.265243	12.978314
c	m^{-1} at m^{-1}	4	3	27 850.523116	-13668.887818	2325.727793	-153.533939	2.762913
c	m^{-1} at m^{-1}	4	4	42861.030876	-25566.868840	5705.288027	-564.277136	20.856037

References

- [1] A.M. García, A.A. Amell, A numerical analysis of the effect of heat recovery burners on the heat transfer and billet heating characteristics in a walkingbeam type reheating furnace, Int. J. Heat Mass Transfer 127 (2018) 1208–1222, http://dx.doi.org/10.1016/j.ijheatmasstransfer.2018.07.121.
- [2] W. Trinks, M.H. Mawhinney, R.A. Shannon, R.J. Reed, J.R. Garvey, Industrial Furnaces, first ed., John Wiley & Sons, 2004.
- [3] L.S. Rothman, I.E. Gordon, R.J. Barber, H. Dothe, R.R. Gamache, A. Goldman, V.I. Perevalov, S.A. Tashkun, J. Tennyson, HITEMP, the high-temperature molecular spectroscopic database, J. Quant. Spectrosc. Radiat. Transfer 111 (15) (2010) 2139–2150, http://dx.doi.org/10.1016/j.jqsrt.2010.05.001.
- [4] R. Yadav, C. Balaji, S.P. Venkateshan, Radiative Heat Transfer in Participating Media, Springer International Publishing, Cham, 2023, http://dx.doi.org/10. 1007/978-3-030-99045-9.
- [5] H.C. Hottel, A.F. Sarofim, Radiative Transfer, McGraw-Hill, New York, 1967.

- [6] M.F. Modest, D.C. Haworth, Radiative Heat Transfer in Turbulent Combustion Systems, Springer International Publishing, Cham, 2016, http://dx.doi.org/10. 1007/978-3-319-27291-7.
- [7] M.F. Modest, The weighted-sum-of-gray-gases model for arbitrary solution methods in radiative transfer, J. Heat Transf. 113 (3) (1991) 650–656, http://dx.doi.org/10.1115/1.2910614.
- [8] M.A. Rajhi, R. Ben-Mansour, M.A. Habib, M.A. Nemitallah, K. Andersson, Evaluation of gas radiation models in CFD modeling of oxy-combustion, Energy Convers. Manage. 81 (2014) 83–97, http://dx.doi.org/10.1016/j.enconman.2014. 02.019.
- [9] F. Cassol, R. Brittes, F.H. França, O.A. Ezekoye, Application of the weighted-sum-of-gray-gases model for media composed of arbitrary concentrations of H2O, CO2 and soot, Int. J. Heat Mass Transfer 79 (2014) 796–806, http://dx.doi.org/10.1016/j.ijheatmasstransfer.2014.08.032.
- [10] J. Guo, L. Shen, X. He, Z. Liu, H.G. Im, Assessment of weighted-sum-of-gray-gases models for gas-soot mixture in jet diffusion flames, Int. J. Heat Mass Transfer 181 (2021) 121907, http://dx.doi.org/10.1016/j.ijheatmasstransfer.2021.121907.
- [11] M. Bahador, B. Sunden, Evaluation of weighted sum of grey gases coefficients for combustion gases using predicted emissivities from high resolution spectroscopic databases, Proc. ASME Turbo Expo (2008) 1791–1799.
- [12] G. Krishnamoorthy, A new weighted-sum-of-gray-gases model for CO2–H2O gas mixtures, Int. Commun. Heat Mass Transf. 37 (2010) 1182–1186, http://dx.doi. org/10.1016/j.icheatmasstransfer.2010.07.007.
- [13] C. Yin, L.C.R. Johansen, L.A. Rosendahl, S.K. Kær, New weighted sum of gray gases model applicable to computational fluid dynamics (CFD) modeling of Oxy–Fuel combustion: Derivation, validation, and implementation, Energy Fuels 24 (12) (2010) 6275–6282, http://dx.doi.org/10.1021/ef101211p.
- [14] R. Johansson, B. Leckner, K. Andersson, F. Johnsson, Account for variations in the H2O to CO2 molar ratio when modelling gaseous radiative heat transfer with the weighted-sum-of-grey-gases model, Combust. Flame 158 (5) (2011) 893–901, http://dx.doi.org/10.1016/j.combustflame.2011.02.001.
- [15] S. Rehfeldt, C. Kuhr, M. Ehmann, C. Bergins, Modeling of radiative properties of an oxyfuel atmosphere with a weighted sum of gray gases for variable carbon dioxide and water vapor concentrations, Energy Procedia 4 (2011) 980–987, http://dx.doi.org/10.1016/j.egypro.2011.01.145.
- [16] T. Kangwanpongpan, F.H. França, R. Da Corrêa Silva, P.S. Schneider, H.J. Krautz, New correlations for the weighted-sum-of-gray-gases model in oxy-fuel conditions based on HITEMP 2010 database, Int. J. Heat Mass Transfer 55 (25–26) (2012) 7419–7433, http://dx.doi.org/10.1016/j.ijheatmasstransfer.2012.07.032.
- [17] L.J. Dorigon, G. Duciak, R. Brittes, F. Cassol, M. Galarça, F.H. França, WSGG correlations based on HITEMP2010 for computation of thermal radiation in non-isothermal, non-homogeneous H2O/CO2 mixtures, Int. J. Heat Mass Transfer 64 (2013) 863–873, http://dx.doi.org/10.1016/j.ijheatmasstransfer.2013.05.010.
- [18] G. Krishnamoorthy, A new weighted-sum-of-gray-gases model for oxy-combustion scenarios, Int. J. Energy Res. 37 (14) (2013) 1752–1763, http://dx.doi.org/10. 1000/cs. 2009
- [19] M.H. Bordbar, G. Wecel, T. Hyppänen, A line by line based weighted sum of gray gases model for inhomogeneous CO2–H2O mixture in oxy-fired combustion, Combust. Flame 161 (9) (2014) 2435–2445, http://dx.doi.org/10.1016/j. combustflame.2014.03.013.
- [20] J. Guo, X. Li, X. Huang, Z. Liu, C. Zheng, A full spectrum k-distribution based weighted-sum-of-gray-gases model for oxy-fuel combustion, Int. J. Heat Mass Transfer 90 (2015) 218–226, http://dx.doi.org/10.1016/j.ijheatmasstransfer. 2015 06 052
- [21] S. Shan, B. Qian, Z. Zhou, Z. Wang, K. Cen, New pressurized WSGG model and the effect of pressure on the radiation heat transfer of H2O/CO2 gas mixtures, Int. J. Heat Mass Transfer 121 (2018) 999–1010, http://dx.doi.org/10.1016/j. iiheatmasstransfer.2018.01.079.
- [22] F.R. Coelho, F.H. França, WSGG correlations based on HITEMP2010 for gas mixtures of H2O and CO2 in high total pressure conditions, Int. J. Heat Mass Transfer 127 (2018) 105–114, http://dx.doi.org/10.1016/j.ijheatmasstransfer. 2018 07 075
- [23] B. Wang, Y. Xuan, An improved WSGG model for exhaust gases of aero engines within broader ranges of temperature and pressure variations, Int. J. Heat Mass Transfer 136 (2019) 1299–1310, http://dx.doi.org/10.1016/j.ijheatmasstransfer. 2019.03.105.
- [24] H. Bordbar, G.C. Fraga, S. Hostikka, An extended weighted-sum-of-gray-gases model to account for all CO2–H2O molar fraction ratios in thermal radiation, Int. Commun. Heat Mass Transfer 110 (2020) 104400, http://dx.doi.org/10.1016/j. icheatmasstransfer.2019.104400.
- [25] X. Wu, W. Fan, S. Liu, J. Chen, H. Guo, Z. Liu, A new WSGGM considering CO in oxy-fuel combustion: A theoretical calculation and numerical simulation application, Combust. Flame 227 (2021) 443–455, http://dx.doi.org/10.1016/j. combustflame.2021.01.022.

- [26] J. Xu, R. Chen, H. Meng, WSGG models for radiative heat transfer calculations in hydrogen and hydrogen-mixture flames at various pressures, Int. J. Hydrog. Energy 46 (61) (2021) 31452–31466, http://dx.doi.org/10.1016/j.ijhydene.2021. 07 040
- [27] Z. Zhou, X. Han, G. Jin, X. Wang, J. Yu, S. Shan, New coefficients of the weighted-sum-of-gray-gases model for gas radiation characteristics of hydrogen/natural gas blends combustion, Int. Commun. Heat Mass Transf. 149 (2023) 107090, http://dx.doi.org/10.1016/j.icheatmasstransfer.2023.107090.
- [28] G. Liu, J. Zhu, Y. Liu, J.-l. Consalvi, F. Liu, A full-spectrum correlated K-distribution based interpolation weighted-sum-of-gray-gases model for CO2-H2O-soot mixture, Int. J. Heat Mass Transfer 210 (2023) 124160, http://dx. doi.org/10.1016/j.ijheatmasstransfer.2023.124160.
- [29] N. Schmitz, L. Sankowski, F. Kaiser, C. Schwotzer, T. Echterhof, H. Pfeifer, Towards CO2-neutral process heat generation for continuous reheating furnaces in steel hot rolling mills – a case study, Energy 224 (2021) 120155, http: //dx.doi.org/10.1016/j.energy.2021.120155.
- [30] A. Peppas, S. Kottaridis, C. Politi, P.M. Angelopoulos, M. Taxiarchou, Multi-model assessment for secondary smelting decarbonisation: The role of hydrogen in the clean energy transition, Hydrogen 4 (2023) 103–119, http://dx.doi.org/10.3390/ hydrogen4010007.
- [31] M. Zier, P. Stenzel, L. Kotzur, D. Stolten, A review of decarbonization options for the glass industry, Energy Convers. Manag.: X 10 (2021) 100083, http: //dx.doi.org/10.1016/j.ecmx.2021.100083.
- [32] S. Mathur, G. Gosnell, B.K. Sovacool, D.D. Del Furszyfer Rio, S. Griffiths, M. Bazilian, J. Kim, Industrial decarbonization via natural gas: A critical and systematic review of developments, socio-technical systems and policy options, Energy Res. Soc. Sci. 90 (2022) 102638, http://dx.doi.org/10.1016/j.erss.2022.102638
- [33] M. Pisciotta, H. Pilorgé, J. Feldmann, R. Jacobson, J. Davids, S. Swett, Z. Sasso, J. Wilcox, Current state of industrial heating and opportunities for decarbonization, Prog. Energy Combust. Sci. 91 (2022) 100982, http://dx.doi.org/10.1016/j.pecs. 2021.100982.
- [34] M.F. Modest, Radiative Heat Transfer, Academic Press, Boston, 2013, http://dx.doi.org/10.1016/C2010-0-65874-3.
- [35] M. Alberti, R. Weber, M. Mancini, Re-creating Hottel's emissivity charts for carbon dioxide and extending them to 40bar pressure using HITEMP-2010 data base, Combust. Flame 162 (3) (2015) 597-612, http://dx.doi.org/10.1016/j. combustflame.2014.09.005.
- [36] M. Alberti, R. Weber, M. Mancini, Re-creating Hottel's emissivity charts for water vapor and extending them to 40 bar pressure using HITEMP-2010 data base, Combust. Flame 169 (2016) 141–153, http://dx.doi.org/10.1016/j. combustflame.2016.04.013.
- [37] R.V. Kochanov, I.E. Gordon, L.S. Rothman, P. Wcisło, C. Hill, J.S. Wilzewski, HITRAN application programming interface (HAPI): A comprehensive approach to working with spectroscopic data, J. Quant. Spectrosc. Radiat. Transfer 177 (2016) 15–30, http://dx.doi.org/10.1016/j.jqsrt.2016.03.005.
- [38] M.F. Modest, S. Mazumder, Radiative heat transfer (Fourth Edition), Academic Press, New York, 2022, http://dx.doi.org/10.1016/B978-0-12-818143-0.00003-1.
- [39] M.F. Modest, H. Zhang, The full-spectrum correlated-k distribution for thermal radiation from molecular gas-particulate mixtures, J. Heat Transf. 124 (1) (2002) 30–38, http://dx.doi.org/10.1115/1.1418697.
- [40] C. Wang, M.F. Modest, T. Ren, J. Cai, B. He, Comparison and refinement of the various full-spectrum k-distribution and spectral line weighted-sum-of-gray-gases models for nonhomogeneous media, J. Quant. Spectrosc. Radiat. Transf. 271 (2021) 107695, http://dx.doi.org/10.1016/j.jqsrt.2021.107695.
- [41] M.K. Denison, B.W. Webb, A spectral line-based weighted-sum-of-gray-gases model for arbitrary RTE solvers, J. Heat Transf. 115 (4) (1993) 1004–1012, http://dx.doi.org/10.1115/1.2911354.
- [42] M.K. Denison, B.W. Webb, The spectral line-based weighted-sum-of-gray-gases model in nonisothermal nonhomogeneous media, J. Heat Transf. 117 (1995) 359–365.
- [43] C. Wang, M.F. Modest, B. He, Improvement of full-spectrum k-distribution method using quadrature transformation, Int. J. Therm. Sci. 108 (2016) 100–107, http://dx.doi.org/10.1016/j.ijthermalsci.2016.05.005.
- [44] G. van Rossum, F.L. Drake Jr., Python reference manual, 1995.
- [45] I. Ansys, Fluent theory guide 5.3.9.1 the weighted-sum-of-Gray-gases model, release R1, 2023.
- [46] T.F. Smith, Z.F. Shen, J.N. Friedman, Evaluation of coefficients for the weighted sum of Gray gases model, J. Heat Transf. 104 (1982) 602–608.